International Journal of Engineering Science 191 (2023) 103899

Contents lists available at ScienceDirect

International Journal of Engineering Science

journal homepage: www.elsevier.com/locate/ijengsci

# Cloaking Rayleigh waves via symmetrized elastic tensors

Z. Chatzopoulos [a], A. Palermo [a,*], A. Diatta [b], S. Guenneau [c,d], A. Marzani [a,*]

[a] Department of Civil, Chemical, Environmental and Materials Engineering, University of Bologna, 40136 Bologna, Italy
[b] Aix-Marseille Universite, CNRS, Centrale Marseille, Institut Fresnel, Avenue Escadrille Normandie-Niemen, 13013, Marseille, France
[c] UMI 2004 Abraham de Moivre-CNRS, Imperial College, London SW7 2AZ, United Kingdom
[d] The Blackett Laboratory, Physics Department, Imperial College, London SW7 2AZ, United Kingdom

ARTICLE INFO

*Keywords:*
Rayleigh waves
Cloaking
Transformation elastodynamics
Symmetrization
Metamaterials

ABSTRACT

In this work we propose a strategy based on coordinate transformation to cloak Rayleigh waves. Rayleigh waves are in-plane elastic waves which propagate along the free surface of semi-infinite media. They are governed by Navier equations that retain their form for an in-plane arbitrary coordinate transformation $\mathbf{x} = \Xi(\mathbf{X})$, upon choosing the specific kinematic relation $\mathbf{U}(\Xi(\mathbf{X})) = \mathbf{u}(\mathbf{x})$ between displacement fields in virtual, i.e. reference, ($\mathbf{U}$) and transformed, i.e. cloaked, ($\mathbf{u}$) domains. However, the elasticity tensor of the transformed domain is no longer fully symmetric, and thus, it is difficult to design with common materials. Motivated by this issue, we propose a symmetrization technique, based on the arithmetic mean, to obtain anisotropic, yet symmetric, elastic tensors for Rayleigh wave near-cloaking. In particular, by means of time-harmonic numerical simulations and dispersion analyses, we compare the efficiency of triangular and semi-circular cloaks designed with the original non-symmetric tensors and the related symmetrized versions. In addition, different coordinate transformations, e.g. linear, quadratic and cubic, are adopted for the semi-circular cloaks. Through the analyses, we show that a symmetrized semi-circular cloak, obtained upon the use of a quadratic transformation, performs better than the other investigated designs. Our study provides a step towards the design of feasible and efficient broadband elastic metamaterial cloaks for surface waves.

## 1. Introduction

Controlling surface waves with architected materials is an open challenge in several engineering applications, ranging from microdevices for electronic components (Jin et al., 2021), like surface acoustic wave (SAW) devices, to meter-sized barriers (Huang & Shi, 2013; Liu, Qin, & Yu, 2020; Liu & Yu, 2022; Meng, Cheng, & Shi, 2020; Muhammad, Lim, & Kamil Żur, 2021; Palermo, Krödel, Marzani, & Daraio, 2016; Pu & Shi, 2018, 2019) and seismic cloaks (Sklan, Pak, & Li, 2018) for ground-borne vibrations. In the latter context, two large-scale experiments recently demonstrated that one can reflect (Brûlé, Javelaud, Enoch, & Guenneau, 2014) or even focus (Brûlé, Javelaud, Enoch, & Guenneau, 2017) surface Rayleigh waves in structured sedimentary soils. These experiments were the result of collaborative work between geotechnical engineers and wave physicists that explored analogies between models of electromagnetic and elastodynamic waves in metamaterials (Colquitt et al., 2014; Dubois et al., 2012; Farhat, Guenneau, & Enoch, 2009; Liu & Zhu, 2019; Stenger, Wilhelm, & Wegener, 2012; Tang et al., 2023; Zareei & Alam, 2017).

Based on those experiments, it was argued that one might build a cloak for Rayleigh waves with concentric layers of structured soil around a building one may wish to protect. Such an approach amounts to considering a physical setup in a plane parallel to the surface. Many numerical works followed, mostly considering the same approach, notably a proposal to reroute Love waves (Palermo,

* Corresponding authors.
*E-mail addresses:* antonio.palermo6@unibo.it (A. Palermo), alessandro.marzani@unibo.it (A. Marzani).

https://doi.org/10.1016/j.ijengsci.2023.103899
Received 6 April 2023; Accepted 18 May 2023
Available online 9 June 2023

2018) in the transverse plane thanks to a graded metasurface, and some conversion of Love waves into downward propagating anti-plane shear bulk waves via a wedge effect in the vertical plane (Maurel, Marigo, Pham, & Guenneau, 2018). In parallel, small-scale experiments on the control of surface seismic waves (Colombi, Roux, Guenneau, Gueguen, & Craster, 2016; Colombi, Zaccherini, Aguzzi, Palermo, & Chatzi, 2020; Palermo et al., 2018) have shown that one can also act upon the deflection of Rayleigh waves in the vertical plane with an array of resonators atop, or buried, in the soil. The corresponding physical setups consider devices acting on a plane orthogonal to the surface.

Following this approach, some authors of this manuscript investigated the cloaking of surface Love waves by transforming the elastic medium along the vertical plane (Chatzopoulos, Palermo, Guenneau, & Marzani, 2022). At first sight, this strategy for cloaking of Love waves should equally work for Rayleigh waves. However, unlike Love waves, which are polarized out-of-plane and can thus be modeled by a scalar Helmholtz equation in the vertical plane, Rayleigh waves are governed by the Navier equations, where the coupling between in-plane pressure and shear waves cannot be avoided.

In this regard, we stress that a major hurdle in Rayleigh wave cloaking is that the Navier equations are not form invariant under an arbitrary geometric transformation (Milton, Briane, & Willis, 2006), leading to non-scalar density and additional third-order elastic tensors in the transformed medium. Notably, Norris and Shuvalov (2011) investigated the relation, e.g. the gauge, between the displacement field of the reference domain and the transformed one and showed that it directly affects the symmetry of the elastic tensor. Recently, 2D elastodynamic cloaking has been approached either by direct design and homogenization of the so-called micropolar metamaterials (Nassar, Chen, & Huang, 2018, 2019, 2020; Wu & Huang, 2022; Zhao, Chen, Chang, & Huang, 2023), which can achieve the required non-symmetric elastic tensor, or by utilizing symmetrization techniques to restore the symmetries of the elastic tensor (Diatta, Kadic, Wegener, & Guenneau, 2016; Sklan et al., 2018). An alternative route to achieve cloaking exploits the use of non-linear elastic pre-stress in hyperelastic material models to relax the constraints on material properties (Barnwell, Parnell, & David Abrahams, 2016; Norris & Parnell, 2012; Parnell, 2012; Parnell & Shearer, 2013; Zhang & Parnell, 2018).

Relevant studies in the context of Rayleigh waves cloaking include the use of micropolar materials to hide a cylinder embedded in the medium (Khlopotin, Olsson, & Larsson, 2015) and near-cloaking techniques to decouple P and S waves (Quadrelli, Craster, Kadic, & Braghin, 2021). Here, we focus, instead, on the use of symmetrized tensors, since micropolar materials can exhibit zero-modes and mechanical instabilities, making them complex to manufacture (Kadic, Bückmann, Stenger, Thiel, & Wegener, 2012). Specifically, our scope is to delve into the effects of symmetrization on the cloaking performance of Rayleigh waves, considering different transformations and cloaking geometries.

To this aim, we organize our manuscript as follows: we first recall the Navier equations for the reference and transformed semi-infinite media. We stress that depending on the choice of the gauge, one can either assume a modified Willis medium, or a Cosserat medium with a non-symmetric elastic tensor.

After adopting the latter, we manipulate its non-symmetric components using the arithmetic mean and assess the effect of symmetrization on the cloaking of Rayleigh waves. Our analysis considers a triangular pinched cloak and 3 types of semi-circular cloaks, distinguished by the adopted radial transformation $C_i$ (linear $C_1$, quadratic $C_2$, cubic $C_3$). The cloaking performance is analyzed by comparing the harmonic wave fields and dispersion relations of ideal, e.g. non-symmetric, and symmetrized cloaks. In particular, the dispersive analysis exploits the inverse participation ratio (IPR), which addresses the localization level of the displacement fields, to identify and count the surface modes of interest.

Next, the performance analysis is continued by means of harmonic simulations and by comparing the transmitted displacement fields after the cloak of symmetrized and ideal cases. We conclude the investigation with a focus on the circular cloaks by examining the requirements for a symmetric elastic tensor for each $C_i$ type of transformation.

## 2. Governing equations for 2-D elasticity

We consider a homogeneous isotropic half-space with material properties $(\lambda, \mu, \rho)$, where $\lambda$ and $\mu$ are the Lamé coefficients and $\rho$ the mass density, respectively, and the spatial coordinates for the reference domain are $\mathbf{X} = (X_1, X_2)$. For in-plane surface waves, i.e. Rayleigh waves, propagating along the horizontal $X_1$ direction, the governing Navier elastodynamic equation reads:

$$\nabla_X \cdot (\mathbf{C} : \nabla_X \mathbf{U}) = \rho \mathbf{U}_{tt} \tag{1}$$

where $\mathbf{C}$ is the isotropic 4th order elasticity tensor, $\mathbf{U} = (U_1, U_2)$ is the displacement and $\mathbf{U}_{tt}$ denotes the second order derivative in time of $\mathbf{U}$. Under the assumption of plane-strain elasticity, the elastic tensor can be written in Voigt's notation $\{1, 2, 6\} = \{11, 22, 12\}$ as:

$$\mathbf{C}_{IJ} = \begin{bmatrix} \lambda + 2\mu & \lambda & 0 \\ \lambda & \lambda + 2\mu & 0 \\ 0 & 0 & \mu \end{bmatrix}, \tag{2}$$

where $I, J = 1, 2, 6$.

We apply a point-wise invertible transformation $\boldsymbol{\Xi}$ that maps the reference configuration (virtual domain) $\mathbf{X} \in \Psi$ to the deformed region (physical domain) as $\mathbf{x} = \boldsymbol{\Xi}(X) \in \psi$ and the remaining domain to itself ($\mathbf{X} \notin \Psi$). As a result, we derive the transformed elasticity tensor in the cloaked region. In Figs. 1$(a)$ – $(d)$, we show two examples of carpet cloaks, a triangular and a semi-circular one, with the related virtual and deformed domains. The transformation gradients for the deformed and the reference domains are

$\mathbf{F} = \nabla_X x$ and $\mathbf{F}^{-1} = \nabla_x X$, respectively. Also, $J = det(\mathbf{F})$ is the determinant of the transformation gradient. Given $\mathbf{x} = \{x_1, x_2\}$ the coordinates for the physical domain, the transformation gradient $\mathbf{F}$ reads:

$$\mathbf{F} = \nabla_X x = \begin{pmatrix} \frac{\partial x_1}{\partial X_1} & \frac{\partial x_1}{\partial X_2} \\ \frac{\partial x_2}{\partial X_1} & \frac{\partial x_2}{\partial X_2} \end{pmatrix} \tag{3}$$

As discussed in the literature, see for example Milton et al. (2006), Eq. (1) is not form invariant upon an arbitrary coordinate transformation $\boldsymbol{\Xi}$ and it depends on the choice of the gauge $\mathbf{U}(\boldsymbol{\Xi}(X)) = \mathbf{A}\mathbf{u}(\mathbf{x})$, where $\mathbf{A}$ is a non-singular matrix. In particular, the choice $\mathbf{A} = \mathbf{F}$ leads to the so-called Willis setting that guarantees symmetric stress tensor (Milton et al., 2006; Norris & Shuvalov, 2011). Despite possessing such a symmetry, a medium that is governed by the Willis equation is difficult to design due to the presence of two additional 3rd order symmetric tensors, which may require the introduction of pre-stresses (Craster, Diatta, Guenneau, & Hutridurga, 2021; Xiang & Yao, 2016). Additionally, in the Willis setting the material density is a 2nd order symmetric tensor, a requirement which can be physically replicated only within narrow frequency bands using resonant microstructures.

For this reason, in the present work, we refrain from using Willis materials and we employ a Cosserat setting. In particular, following the idea by Norris and Shuvalov (2011), by assuming the gauge $\mathbf{U}(\boldsymbol{\Xi}(\mathbf{X})) = \mathbf{u}(\mathbf{x})$ ($\mathbf{A} = \mathbf{I}$) for the displacements (Brun & Guenneau, 2023; Brun, Guenneau, & Movchan, 2009), we derive the governing equation in the physical domain $\mathbf{x} = (x_1, x_2)$ as:

$$\nabla_x \cdot (\mathbf{C}^{eff} : \nabla_x \mathbf{u}) = \rho^{eff} \mathbf{u}_{tt} \tag{4}$$

where

$$\begin{aligned} C^{eff}_{ijkl} &= J^{-1} C_{IjKl} F_{iI} F_{kK} \\ \rho^{eff} &= \rho J^{-1} \end{aligned} \tag{5}$$

are the transformed mechanical parameters of the cloaked region (purple region in Fig. 1b and blue region in Fig. 1d) in Einstein summation. As a result, the transformed elasticity tensor $C^{eff}$ preserves the major symmetries ($C^{eff}_{ijkl} = C^{eff}_{klij}$, etc.), but does not possess the minor ones as:

$$C^{eff}_{ijkl} \neq C^{eff}_{jikl} \neq C^{eff}_{ijlk} \neq C^{eff}_{jilk} \tag{6}$$

except for very special cases such as in the framework of conformal transformations. Nonetheless, the medium can still be described by a single 4th-order non-symmetric and, eventually, inhomogeneous elastic tensor.

## 3. Carpet cloaking for Rayleigh waves: Transformation

Due to the vectorial nature of Rayleigh waves, cloaking has been hindered by the requirement of a material with non-symmetric elasticity tensor. Indeed, several researchers (Chen, Nassar, & Huang, 2021; Frenzel, Kadic, & Wegener, 2017; Zhang, Chen, Liu, & Hu, 2020; Zhao et al., 2023) have proposed metamaterials that can obtain the non-symmetric behavior required for cloaking. Here, however, we focus our investigation on a different aspect, aiming at analyzing and comparing different linear and non-linear transformations, as well as symmetrization strategies, to obtain an easy-to-realize, well-performing, symmetric cloaks for Rayleigh waves. Specifically, we delve into the behavior of carpet cloaks with boundaries described by either linear functions (triangular shape) or semi-circular ones.

### 3.1. Triangular carpet cloak

We first consider a two-dimensional carpet cloak of triangular shape. Given a set of cartesian coordinates centered along the cloak symmetry axis ($\mathbf{X} = \{X_1, X_2\}$, $\mathbf{x} = \{x_1, x_2\}$), we denote with $z_1(x_1)$ and $z_2(x_1)$ the interior and exterior boundaries of the cloak, respectively. The transformation $\boldsymbol{\Xi}^T$ that maps the region enclosed between two curves $(X_1; 0)$ and $(X_1; z_2(X_1))$ of the virtual domain, Fig. 1a, to the one comprised between $(x_1; z_1(x_1))$ and $(x_1; z_2(x_1))$ of the real domain, Fig. 1b, is:

$$\boldsymbol{\Xi}^T : \begin{cases} x_1 = X_1 \\ x_2 = (\frac{z_2(X_1) - z_1(X_1)}{z_2(X_1)}) X_2 + z_1(X_1) \end{cases} \tag{7}$$

Note that $(X_1; 0)$ is mapped on $(x_1; z_1(x_1))$ while $(X_1; z_2(X_1))$ is point-wise fixed. Let $z_1(x_1) = \frac{a}{c}|x_1| - a$ and $z_2(x_1) = \frac{b}{c}|x_1| - b$ be piece-wise linear curves, where $a, b, c$ are the geometric parameters of the cloak, as illustrated in Fig. 1b. Then, using Cartesian $\mathbf{X} = \{X_1, X_2\}$, $\mathbf{x} = \{x_1, x_2\}$ coordinates the Jacobian of the transformation reads:

$$\mathbf{F}^T = \begin{bmatrix} \frac{\partial x_1}{\partial X_1} & \frac{\partial x_1}{\partial X_2} \\ \frac{\partial x_2}{\partial X_1} & \frac{\partial x_2}{\partial X_2} \end{bmatrix} = \begin{bmatrix} 1 & 0 \\ F_{21}(x_1) & F_{22} \end{bmatrix} \tag{8}$$

where $F_{21}(x_1) = sign(x_1)\frac{a}{c}$ and $F_{22} = det(\mathbf{F}^T) = \frac{b-a}{b}$. According to Eq. (5) and adopting the augmented Voigt notation for the plane problem as $\{1, 2, 6, \bar{6}\} = \{11, 22, 12, 21\}$, we obtain the following transformed elastic tensor and material density properties within

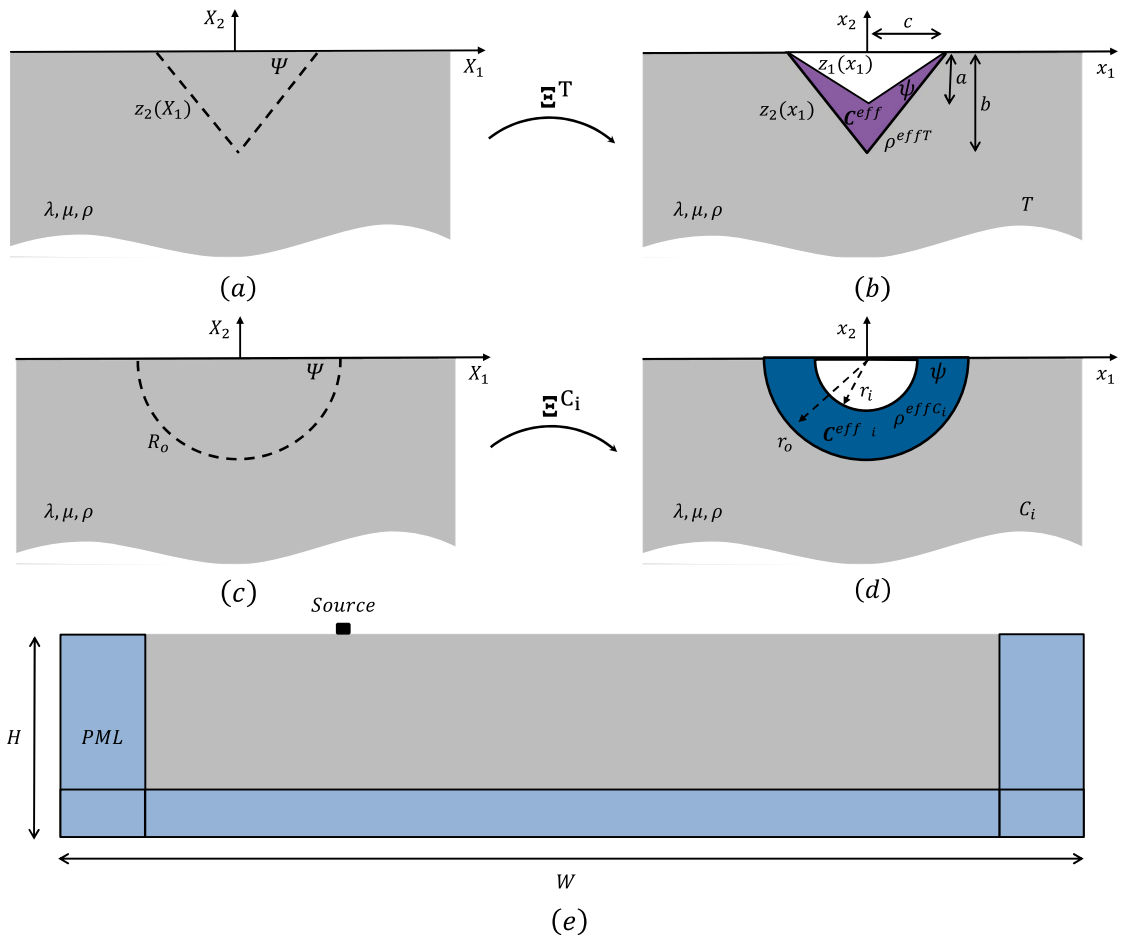


**Fig. 1.** (*a*) Reference configuration (virtual domain) of the triangular cloak. (*b*) Deformed configuration (physical domain) obtained by the action of ($\Xi^T$) that maps the (virtual domain) into a defect (white region) surrounded by the cloak (purple region). (*c*) Reference configuration (virtual domain) of the semi-circular cloak. (*d*) Deformed configuration (physical domain) obtained by the action of ($\Xi^{C_i}$) that maps the (virtual domain) into a defect (white region) surrounded by the cloak (blue region). (*e*) Schematic representation of the FEM model.

the cloak domain:

$$\mathbf{C}_{IJ}^{effT} = \begin{bmatrix} \frac{\lambda+2\mu}{F_{22}} & \lambda & 0 & \frac{F_{21}(x_1)}{F_{22}}(\lambda+2\mu) \\ \lambda & \frac{F_{21}(x_1)^2\mu+F_{22}^2(\lambda+2\mu)}{F_{22}} & \frac{F_{21}(x_1)}{F_{22}}\mu & F_{21}(x_1)(\lambda+\mu) \\ 0 & \frac{F_{21}(x_1)}{F_{22}}\mu & \frac{\mu}{F_{22}} & \mu \\ \frac{F_{21}(x_1)}{F_{22}}(\lambda+2\mu) & F_{21}(x_1)(\lambda+\mu) & \mu & \frac{F_{21}(x_1)^2(\lambda+2\mu)+F_{22}^2\mu}{F_{22}} \end{bmatrix}, \quad \rho^{effT} = \rho F_{22}^{-1} \tag{9}$$

for $I, J = 1, 2, 6, \bar{6}$. Note that the effective density is constant. As anticipated in the previous section, the elastic tensor of Eq. (9) is non-symmetric. In particular, it has 3 non-symmetric entries, which in the augmented Voigt notation read:

$$\begin{cases} C_{16}^{effT} \neq C_{1\bar{6}}^{effT} \\ C_{26}^{effT} \neq C_{2\bar{6}}^{effT} \\ C_{66}^{effT} \neq C_{6\bar{6}}^{effT} \neq C_{\bar{6}\bar{6}}^{effT} \end{cases} \tag{10}$$

### 3.2. Circular carpet cloak

We now consider the case of annulus shaped semi-circular cloaks located at the free-surface of the semi-infinite domain (Fig. 1d). To simplify the definition of the transformed mechanical properties, we introduce a set of polar coordinates $\mathbf{X} = \{R, \Theta\}$ centered within the cloaked domain, where $R = \sqrt{{X_1}^2 + {X_2}^2}$ and $\Theta = \arctan \frac{X_2}{X_1}[\pi]$, where $[\pi]$ specifies the branch cut taken for arctan.

For such a configuration, we consider and compare 3 different types of radial transformations $\Xi^{C_i} : (R, \Theta) \rightarrow (r, \theta)$ that map the origin (0,0) of the reference system, Fig. 1c, onto an inner circle of radius $r_i = a$ in the physical one, and the outer circle $R_o = r_o = b$ to itself (see Fig. 1d):

$$\Xi^{C_1} : \begin{cases} r = \frac{b-a}{b} R + a \quad 0 \le R \le R_o \\ \theta = \Theta \end{cases} \tag{11}$$

$$\Xi^{C_2} : \begin{cases} r = A_2 R^2 + A_1 R + A_0 \quad 0 \le R \le R_o \\ \theta = \Theta \end{cases} \tag{12}$$

where:

$$A_2 = \frac{a}{b^2}, \quad A_1 = \frac{b - 2a}{b}, \quad A_0 = a. \tag{13}$$

$$\Xi^{C_3} : \begin{cases} r = B_3 R^3 + B_2 R^2 + B_1 R + B_0 \quad 0 \le R \le R_o \\ \theta = \Theta \end{cases} \tag{14}$$

where:

$$B_3 = \frac{2a}{b^3}, \quad B_2 = \frac{-3a}{b^2}, \quad B_1 = 1, \quad B_0 = a. \tag{15}$$

The general form of the Jacobian of such transformation in polar basis reads:

$$\mathbf{F}^C = \begin{bmatrix} \frac{\partial r}{\partial R} & \frac{\partial r}{R \partial \Theta} \\ \frac{r \partial \theta}{\partial R} & \frac{r \partial \theta}{R \partial \Theta} \end{bmatrix} \tag{16}$$

Specifically, for each transformation $C_i$ in Eqs. (11), (12), (14) we obtain:

$$\mathbf{F}^{C_1} = \begin{bmatrix} F_{11}^{C_1} & 0 \\ 0 & F_{22}^{C_1} \end{bmatrix} = \begin{bmatrix} \frac{(b-a)}{b} & 0 \\ 0 & \frac{(b-a)}{(r-a)} \frac{r}{b} \end{bmatrix} \tag{17}$$

$$\mathbf{F}^{C_2} = \begin{bmatrix} F_{11}^{C_2} & 0 \\ 0 & F_{22}^{C_2} \end{bmatrix} = \begin{bmatrix} \frac{\sqrt{b^2 - 4ab + 4ar}}{b} & 0 \\ 0 & \frac{2ar}{2ab - b^2 + b\sqrt{b^2 - 4ab + 4ar}} \end{bmatrix} \tag{18}$$

$$\mathbf{F}^{C_3} = \begin{bmatrix} F_{11}^{C_3} & 0 \\ 0 & F_{22}^{C_3} \end{bmatrix} = \begin{bmatrix} \frac{6aR^2(r)}{b^3} - \frac{6aR(r)}{b^2} + 1 & 0 \\ 0 & \frac{r}{R(r)} \end{bmatrix} \tag{19}$$

where:

$$R(r) = \frac{b}{2} + \frac{\frac{b^2}{4} - \frac{b^3}{6a}}{\left( \sqrt{\left( \frac{a b^3 - b^3 r}{4a} - \frac{b^3}{8} + \frac{b^4}{8a} \right)^2 - \left( \frac{b^2}{4} - \frac{b^3}{6a} \right)^3} - \frac{a b^3 - b^3 r}{4a} + \frac{b^3}{8} - \frac{b^4}{8a} \right)^{1/3}} + \left( \sqrt{\left( \frac{a b^3 - b^3 r}{4a} - \frac{b^3}{8} + \frac{b^4}{8a} \right)^2 - \left( \frac{b^2}{4} - \frac{b^3}{6a} \right)^3} - \frac{a b^3 - b^3 r}{4a} + \frac{b^3}{8} - \frac{b^4}{8a} \right)^{1/3}. \tag{20}$$

We remark that the above transformations are singular, since they map the origin (a point) into a circle of radius $r_i$. The proper approach to avoid such singularities requires considering a very small circle of radius $\epsilon$ instead of the origin (Kohn, Lu, Schweizer, & Weinstein, 2014). The reader can find a more detailed discussion concerning the offset parameter $\epsilon$ in Appendix.

Additionally, we underline that the parameters $A_i$, $B_i$ in $C_2$ and $C_3$ types of transformations, respectively, are obtained from the traction continuity requirement on the outer boundary i.e. $\frac{\partial r}{\partial R}(R_o) = 1$, since the surrounding space of $\Psi$ is mapped onto itself. In contrast, this requirement is not satisfied in the $C_1$ transformation.

At this stage, using the augmented Voigt notation for the plane-strain problem in polar coordinates: $\{1,2,6,\bar{6}\} = \{rr,\theta\theta,r\theta,\theta r\} = \{11,22,12,21\}$, we obtain the following effective properties for any type of transformation ($i = 1,2,3$):

$$\mathbf{C}_{IJ}^{eff C_i} = \begin{bmatrix} \frac{F_{11}^{C_i}}{F_{22}^{C_i}}(\lambda+2\mu) & \lambda & 0 & 0 \\ \lambda & \frac{F_{22}^{C_i}}{F_{11}^{C_i}}(\lambda+2\mu) & 0 & 0 \\ 0 & 0 & \frac{F_{11}^{C_i}}{F_{22}^{C_i}}\mu & \mu \\ 0 & 0 & \mu & \frac{F_{22}^{C_i}}{F_{11}^{C_i}}\mu \end{bmatrix}, \quad \rho^{eff C_i} = \frac{\rho}{det(\mathbf{F}^{C_i})} \tag{21}$$

for $I,J = 1,2,6,\bar{6}$. Again, the elastic tensor presents non-symmetric components:

$$C_{66}^{eff C_i} \neq C_{6\bar{6}}^{eff C_i} \neq C_{\bar{6}6}^{eff C_i} \tag{22}$$

Hence, compared to the triangular-shaped cloak, the circular one presents a reduced number of non-symmetric elastic tensor components. In what follows, we discuss and show how this feature impacts the performance of symmetrized cloaks.

## 4. Carpet cloaking for Rayleigh waves: Symmetrization

The symmetrization of an elastic tensor is a simple, yet effective, strategy to approximate the non-symmetric constitutive behavior of an "ideal" cloak with a standard Cauchy-type material, easily realizable with common media. Different symmetrization strategies, such as geometric (Sklan et al., 2018) or arithmetic (Diatta et al., 2016) means have already been explored to realize feasible cloaks for bulk and flexural waves. In this study, we build upon a recent work proposed by Craster et al. (2021), where it is shown that a symmetric tensor $\mathbf{C}^{Sym}$ obtained from the arithmetic mean nullifies the variational problem:

$$min_{\mathbf{A}\in M}|((\mathbf{C}^{eff} - \mathbf{C}^{Sym}) : \mathbf{A}) : \mathbf{A}| = 0 \tag{23}$$

where $M$ stands for the space of symmetric square matrices. In other words, the elastic energy per unit volume due to strain remains unchanged upon replacing the transformed Cosserat material ($C^{eff},\rho$) by the corresponding approximated Cauchy material ($C^{Sym},\rho$).

Our strategy is to choose the tensor components in such a way that the constraints above are satisfied, whilst keeping the remaining entries unaltered. For the triangular cloak, the requirements for a symmetric elastic tensor are:

$$\begin{cases} C_{16}^{Sym} = C_{1\bar{6}}^{Sym} \\ C_{26}^{Sym} = C_{2\bar{6}}^{Sym} \\ C_{66}^{Sym} = C_{6\bar{6}}^{Sym} = C_{\bar{6}6}^{Sym} \end{cases} \tag{24}$$

Then, from Eqs. (23)–(24) we have:

$$\begin{aligned} |((\mathbf{C}^{effT} - \mathbf{C}^{Sym}) : \mathbf{A}) : \mathbf{A}| = |(C_{16}^{eff} + C_{1\bar{6}}^{eff} + C_{\bar{6}1}^{eff} + C_{\bar{6}\bar{1}}^{eff} - 4C_{16}^{Sym})A_{11}A_{12} \\ +(C_{26}^{eff} + C_{2\bar{6}}^{eff} + C_{\bar{6}2}^{eff} + C_{\bar{6}\bar{2}}^{eff} - 4C_{26}^{Sym})A_{22}A_{12} + (C_{66}^{eff} + C_{6\bar{6}}^{eff} + C_{\bar{6}6}^{eff} + C_{\bar{6}\bar{6}}^{eff} - 4C_{66}^{Sym})A_{12}^2| \end{aligned} \tag{25}$$

Conversely, for the circular cloaks $C_i$ ($i = 1,2,3$) we get the condition:

$$C_{66}^{Sym} = C_{6\bar{6}}^{Sym} = C_{\bar{6}6}^{Sym} \tag{26}$$

In similar fashion, using Eq. (26) we obtain:

$$|((\mathbf{C}^{eff C_i} - \mathbf{C}^{Sym}) : \mathbf{A}) : \mathbf{A}| = |(C_{66} + C_{6\bar{6}} + C_{\bar{6}6} + C_{\bar{6}\bar{6}} - 4C_{66}^{Sym})A_{12}^2| \tag{27}$$

i.e. the variational problem is equal to zero if we choose the function $C_{IJ}^{Sym} = \frac{C_{IJ}^{eff}+C_{I\bar{J}}^{eff}+C_{\bar{I}J}^{eff}+C_{\bar{I}\bar{J}}^{eff}}{4}$ for $I,J = 1,2,6$, where: $\{1,2,6,\bar{6}\} = \{11,22,12,21\}$.

Regarding the symmetrization approach and the related design of composite materials matching the symmetrized effective properties, we remark that the set of possible (symmetric) effective elasticity tensors of composites built from two materials with isotropic elasticity tensors has been studied in a number of papers, see e.g. Milton (2002) for a review. Additionally, if one restricts the analysis to mechanical metamaterials consisting of two phases, one of which being void, then microgeometries within the elementary cells can be found in Milton, Briane, and Harutyunyan (2017); these would be good candidates to design the metamaterial cloak. Conversely, it is possible to follow a different route avoiding the symmetrization and approximating the elasticity tensor without the minor-symmetries with chiral elastic metamaterials. However, the latter approach cannot achieve the required effective elasticity tensor over a finite bandwidth.

## 5. Numerical results and comparisons

We analyze the propagation of Rayleigh waves in a homogeneous half-space hosting a triangular or semi-circular shaped defect. For both configurations, the cloak mechanical parameters are obtained according to the geometrical transformation in Eq. (7) and Eqs. (11)–(14). For the numerical example, we consider a material density $\rho = 1600\ \mathrm{kg/m^3}$, shear and pressure velocities equal to $c_s = 300$ m/s and $c_p = \sqrt{3}c_s$, respectively.

We introduce the following normalized quantities to ease and generalize the discussion of the results:

- Normalized wavelength $\lambda^\star = b$, so that $k^\star = \frac{2\pi}{\lambda^\star}$, i.e. we normalize with respect to a wavelength which is equal to the depth of the cloak.
- Normalized frequency $f^\star = \frac{c_R}{\lambda^\star}$, where $c_R$ is Rayleigh wave velocity, which can be approximated by the following formula: $c_R = c_s \frac{0.826+1.14\nu}{1+\nu}$ where $\nu$ is the Poisson's ratio.

To assess the cloaking abilities, we perform time-harmonic simulations using the finite element software COMSOL Multiphysics. We begin by modeling a 2D domain of dimensions $W \times H$ (Fig. 1e). The dimensions of the model are chosen as $W = 12.5\lambda^\star$ and $H \approx 4.305\lambda^\star$.

The bottom of the half-space model is fixed, the surface is stress-free, and Perfectly Matched Layers are used to diminish reflections from the model boundaries. Rayleigh waves are generated by a surface point source located at $0.35W$ from the left edge of the model. The triangular-shaped inclusion has length $a = 0.0774H$ and width $2c = 0.309H$, and is surrounded by a cloak of related shape that extends along the depth of $b = 3a = 0.232H$. The semicircular defect has radius $a$ and its adjoined cloak has radius $b$.

### 5.1. Ideal cloaks

We begin our investigation by analyzing the performance of the "Ideal Cloaks", namely domains with mechanical parameters defined according to the transformation in Eq. (5). Our aim is to verify that such Cosserat (non-symmetric) cloak can perfectly hide a surface defect from the propagation of Rayleigh waves in a broadband frequency range.

To this purpose, time-harmonic simulations are performed in order to compare the surface displacement field of the system in (i) the pristine configuration, i.e., the domain with no defect ("Reference"), (ii) the domain with the defect ("Obstacle"), and (iii) the domain with the cloaked defect ("Ideal Cloak"). In particular, we display the fields as computed for harmonic excitation at $f^\star = [1, 2]$ in Fig. 2. The results for the pinched triangular $T$ and semi-circular cloaks $C_i$ at both selected frequencies verify that the displacement field of the reference configuration (Fig. 2($a$) and ($b$)) is almost perfectly approximated by the case with the ideal (non-symmetric) cloak (Figs. 2($c$)–($f$)), as the waves are smoothly detoured around the obstacle. The performance of the cloaks is better understood by comparing the cloaked wave fields with those obtained in the uncloaked scenarios (see Figs. 2($g$)–($j$)). In the latter, scattering effects dominate the field around the cloak and lead to the generation of bulk waves. To generalize these results, we calculate the normalized transmitted displacement field $\frac{\langle u \rangle}{\langle u_{Ref} \rangle}$, namely the ratio between the average surface displacement $\langle u \rangle$ computed beyond the obstacle for the ideal cloaks and the obstacle cases, and the same average displacement computed for the reference configuration $\langle u_{Ref} \rangle$. The results, depicted in Fig. 2$k$, indicate perfect performance of the ideal cloaks ($\frac{\langle u \rangle}{\langle u_{Ref} \rangle} \approx 1$), whereas the cases of a defect without the cloaking device are unable to provide adequate efficiency since the transmitted surface field is highly reduced compared to the reference.

For a more complete description of the capabilities of the cloak, we compare the dispersive properties of Rayleigh waves propagating along a homogeneous reference medium and along the cloaked setting. Here, our scope is to prove that a cloak with effective properties given by Eqs. (9) or (21) is able to fully duplicate the properties of the pristine homogeneous medium in a broadband range of frequencies. Thus, for both the triangular and semi-circular defects, we investigate a small portion (unit cell) of the 2D medium enclosing the analyzed cloaks. The unit cells have dimension $H \times L_c$ (see top of Figs. 3($a$)–($b$)) and are modeled with FE using COMSOL Multiphysics. To obtain the dispersive properties of surface elastic waves propagating in such media, we impose fixed boundary conditions at the bottom surface of the cell, and Bloch boundary conditions along the $x_1$ direction. Note that, as in Chatzopoulos et al. (2022), the transformation for the triangular carpet cloak is invariant along the $x_1$ direction and thus the unit cell can be chosen with no particular restrictions on its lenght. The dispersion curve is then computed by varying the wavenumber inside the first Brillouin zone of interest, $k_{x_1} = [\frac{\pi}{100L_c}; \frac{\pi}{L_c}]$. In contrast, for radial transformations discussed in this work, a unit cell of dimension smaller than the dimension of the cloak ($L_c < r_o = b$) subjected to Bloch boundary conditions along the $x_1$ direction leads to overlapping transformation. In this regard, Meirbekova and Brun (2020) recently showed that in such scenario discrepancies arise in the dispersive properties due to the intersection of the cloak with the boundary of the unit cell. Hence, to avoid this phenomenon, the unit cell must be at least the size of the cloak (we choose $L_c = 2.1r_o$). However, the above restriction on the dimension of the unit cell narrows the size of the first Brillouin zone (which is inversely proportional to the unit cell length) and forces the calculation of multiple modes (>500) for each wavenumber to compute frequencies up to $f^\star = 2.5$. Among these, only a small portion of them represent waves confined at the surface (in particular, in a homogeneous medium, there exists only a Rayleigh mode). The problem is thus shifted into the collection/recognition of such surface modes among the plethora of wave solutions computed with a finite cell. For this purpose, we utilize the inverse participation ratio (IPR) (Evers & Mirlin, 2000; Monthus & Garel, 2010; Murphy, Wortis, & Atkinson, 2011; Tsukerman, 2017; Wegner, 1980), computed in terms of the displacements, according to the relation:

$$IPR = \frac{\iint_{\psi^\star} \|\mathbf{u}\|^4 \, dx_1 \, dx_2}{\left(\iint_{\psi^\star} \|\mathbf{u}\|^2 \, dx_1 \, dx_2\right)^2} |\psi^\star| \tag{28}$$

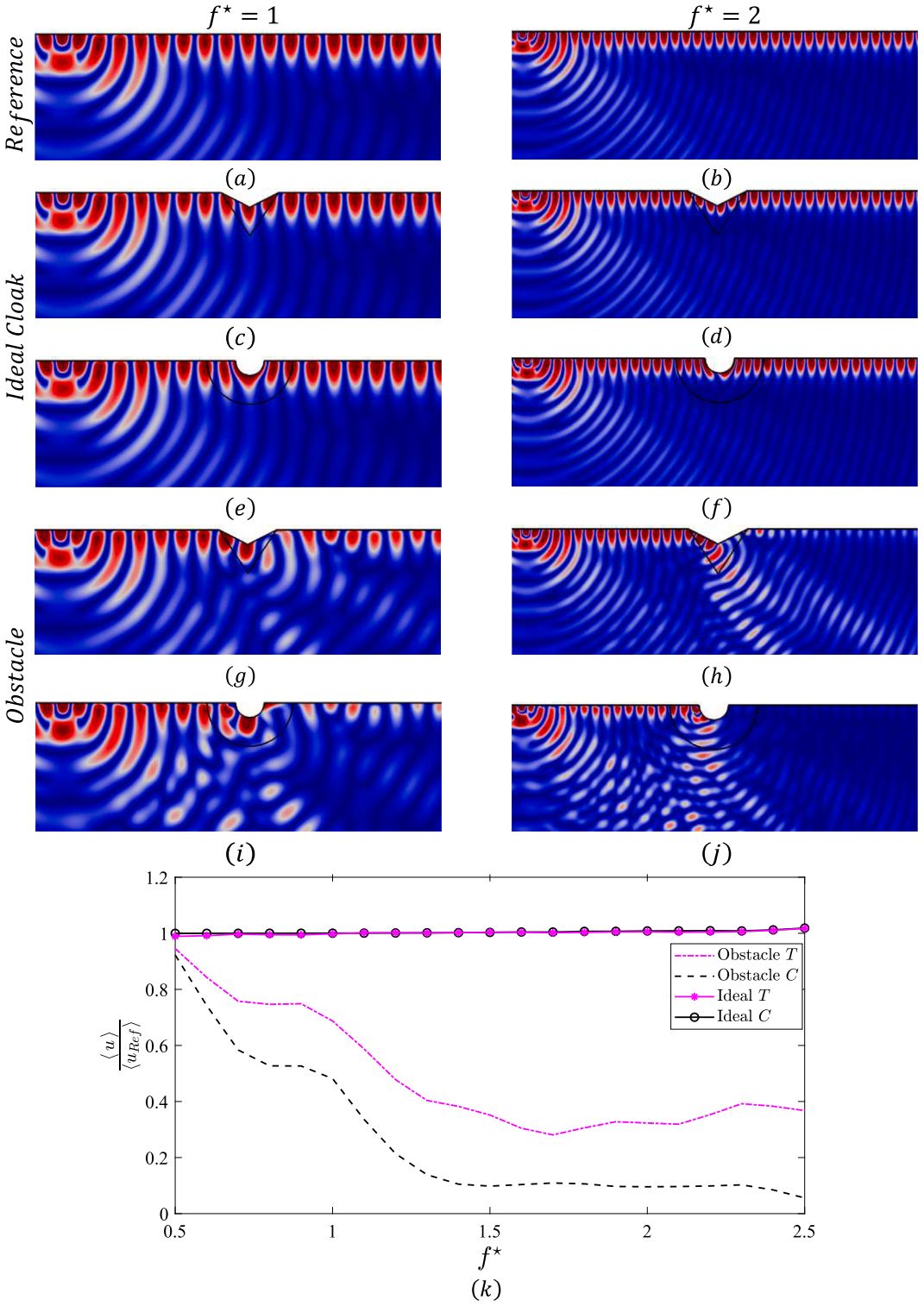


**Fig. 2.** Displacement fields for the Reference $(a)-(b)$, Ideal Cloak $(c)-(f)$ and Obstacle $(g)-(j)$ configurations, of the triangular $T$ and the circular $C_i$ type of cloaks, computed at frequencies $f^\star = [1, 2]$, respectively. $(k)$ Performance of the ideal cloaks and the obstacle cases, computed by using the average of the total displacement of the transmitted field along the surface beyond the cloaked region.

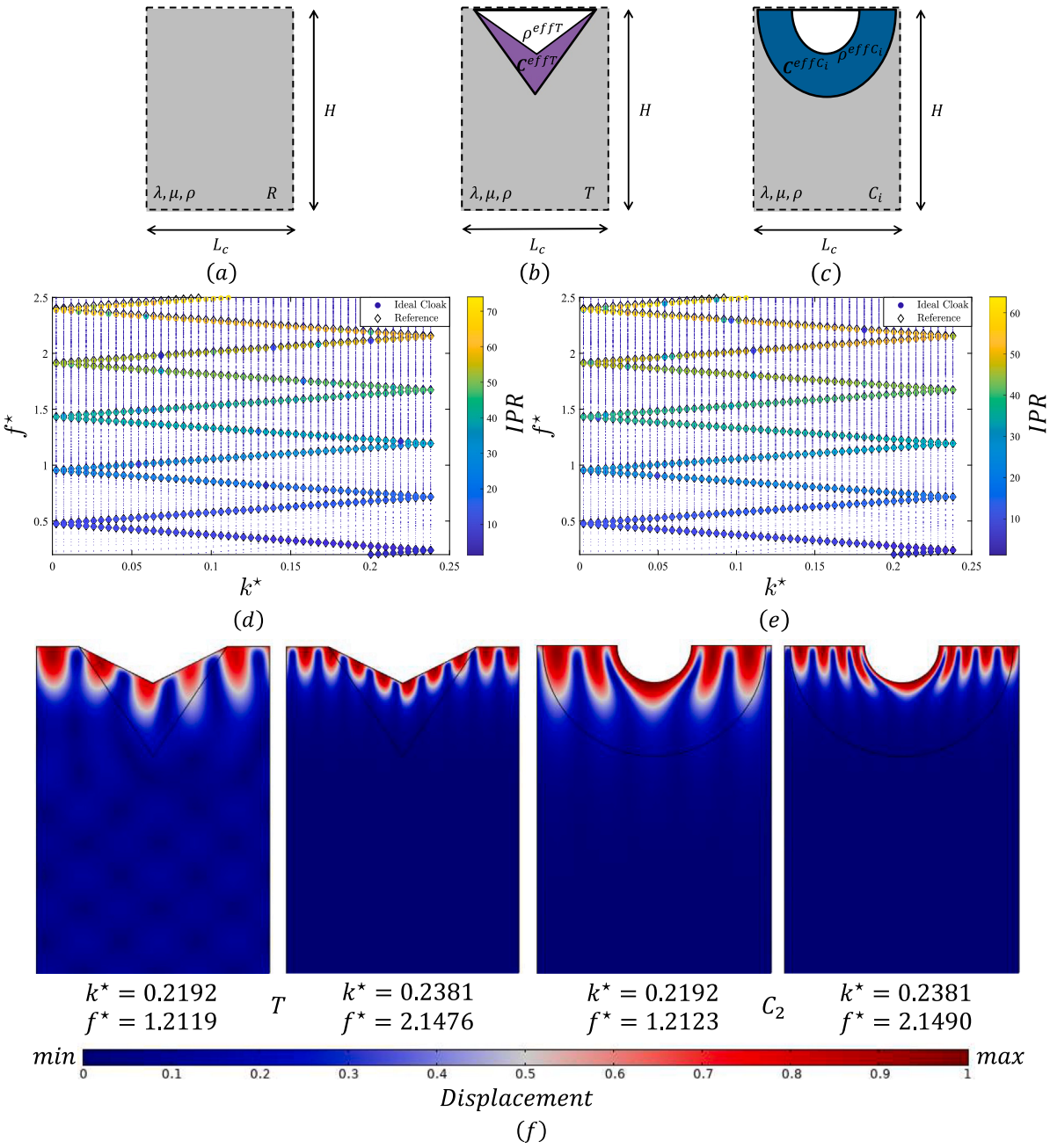


**Fig. 3.** Schematics of the unit cells for the (*a*) reference $R$, (*b*) triangular $T$ and (*c*) circular $C_i$ cloak configurations, respectively. (*d*)-(*e*) Dispersion curves for the reference (diamond dots) and the ideal cloaks (contour circle dots) configurations, respectively. (*f*) Snapshots of surface modes displacement field, as obtained for the triangular $T$ (left) and the circular $C_2$ (right) ideal cloaks, respectively.

where we normalize the ratio by multiplying it with the area of the model $|\psi^\star|$ and $\|\mathbf{u}\| = \sqrt{u_1^2 + u_2^2}$ is the total displacement. The IPR has been used extensively in solid state physics to measure the localization of particles-atoms over a domain. In our context, the IPR measures the localization of the displacement field which will occur at the free-surface for the domain of interest; in practice, the larger the IPR the higher is the localization of the displacement field.

For our example, an IPR $> 3.5$ allows us to clearly distinguish surface modes from bulk ones. In Figs. 3$(d)-(e)$ we display with colored dots (based on the IPR values) the surface wave modes traveling within the triangular and semicircular cloak, respectively. The remaining bulk modes (IPR $< 3.5$) are marked in the background by smaller gradually sized dots. The reader can appreciate the matching between Rayleigh modes within the cloaked domains and the Rayleigh solutions within the reference field, which

**Table 1**
Average value of the ratio $\frac{F^{C_i}_{11}}{F^{C_i}_{22}}$ of each symmetrized circular cloak.

| Transformation | $\langle D^{C_i} \rangle$ |
|---|---|
| $C_1$ | 0.45069 |
| $C_2$ | 0.63 |
| $C_3$ | 0.4527 |

demonstrate the broadband cloaking capabilities of the analyzed non-symmetric cloaks. As an example, surface modes pertaining to two wavenumber solutions ($k^\star = [0.2192, 0.2381]$) for each of the $T$ and $C_2$ cloaks are portrayed in Fig. 3$f$.

### 5.2. Symmetrized cloaks

In what follows, we delve into the behavior of symmetrized cloaks with triangular $T$ and semi-circular $C_i$ transformations. Our scope is to find which combination of symmetrization/cloak geometry provides the best cloaking performance. The displacement field of harmonic solutions for the symmetrized cloaks at frequencies $f^\star = [1, 2]$ are displayed in Figs. 4$(a)-(h)$. For $f^\star = 1$, all the investigated symmetric cloaks are unable to efficiently reroute the wavefield around the defect (see Figs. 4$(a), (c), (e), (g)$) and have a response similar to the "Obstacle" case (Figs. 2$(g)$ and $(i)$). Conversely, at frequency $f^\star = 2$ the symmetric cloaks are able to better reroute the wavefield around the obstacle (see Figs. 4$(b), (d), (f)$ and $(h)$). To quantify the performance of the cloak over a broader frequency range, we compute again the normalized average transmitted field $\frac{\langle u_{Sym} \rangle}{\langle u_{Ideal} \rangle}$ along the domain's surface after the cloak. Here, the surface displacement field is normalized by the field of the ideal case. The ratio $\frac{\langle u_{Sym} \rangle}{\langle u_{Ideal} \rangle}$ versus the frequency of excitation is reported in Fig. 4$i$ for all the considered symmetric cloaks. For $f^\star = 0.5$, all cases have similar behavior, since the wavelength is too long compared to the dimension of the cloak. Furthermore, all the cloaks show a performance drop at around $f^\star = 1$, where the wavelength is equal to the size of the cloak. In particular, for the triangular inclusion, the uncloaked obstacle transmits more energy than symmetrized cloak until frequencies at around $f^\star = 1.4$. The poorer performance of the triangular-shaped cloak with respect to the circular ones, can be possibly attributed to the larger number of conditions (3) required for its symmetrization, as compared to the circular one (1), as shown in Eqs. (24) and (26). Better cloak efficacy is obtained in the higher frequency regime, i.e. when $f^\star > 1.5$, with a peak performance around $f^\star = 2$. Overall, from Fig. 4$i$, it is clear that the $C_2$ transformation provides the best performance compared to $C_1$ and $C_3$.

To better appreciate the above results, we replicate the dispersive analysis with unit cells consisting of symmetrized cloaks. The results are depicted in Fig. 5. It is evident that up to $f^\star = 0.75$, the dispersive properties of the symmetrized cloak match the ones of the reference, since at those frequencies the wavelength is small compared to the dimension of the cloak. In addition, the $C_2$ transformation (Fig. 5$c$) shows the highest number of surface modes, 417 out of the 520 of the ideal case in Figs. 3$(d)$ and $(e)$, followed by 388 modes in the triangular pinched cloak $T$ (Fig. 5$a$), 370 modes in $C_1$ (Fig. 5$b$) and 296 modes in $C_3$ (Fig. 5$d$) upon the same IPR value. This is a further indication of the better performance of the $C_2$ cloak. The reader can find examples of such localized surface modes obtained for symmetrized $T$ and $C_2$ cloaks in Fig. 5$e$.

To further support the premise that the $C_2$ transformation presents better performance with respect to other ones, we notice that from Eqs. (21) and (26) the approximation of the symmetrized circular cloak depends on the ratio $D^{C_i} = \frac{F^{C_i}_{11}}{F^{C_i}_{22}}$. A value of $D^{C_i} = 1$ represents a scenario where the ideal tensor is symmetric, namely a scenario where symmetrization is not required. Note that, according to Milton et al. (2006) this cannot be achieved with our choice of gauge. Nonetheless we can rank the level of minor symmetry breaking introduced by the different transformation by using the ratio $D^{C_i}$.

Since $D^{C_i}$ varies along the radial coordinate, we compute its mean value along the radial direction of the cloak as:

$$\langle D^{C_i} \rangle = \frac{1}{r_{cloak}} \int_{r_{cloak}} D^{C_i} dr \tag{29}$$

where $r_{cloak} = r_o - r_i = b - a$ is the radial length of the cloak. The results obtained for the 3 types of transformations $C_i$ are collected in Table 1:

As expected, the $D^{C_2}$ is higher than the analogous ratio computed for the linear $C_1$ and cubic transformation $C_3$, thus indicating a lower deterioration of the performance upon symmetrization.

## 6. Conclusion

In this study, we investigated the cloaking of Rayleigh waves by means of cloaks with symmetrized elastic tensors. Since the Navier elastodynamic equation is not form-invariant for in-plane surface waves, we assumed a Cosserat gauge for the displacements to recover the form invariance of the governing equation. However, this step comes at the cost of demanding a material with effective properties that do not satisfy the minor symmetries of the elasticity tensor. For this reason, our strategy relied on the symmetrization of the elasticity tensor using the arithmetic mean. In particular, we examined the performance of cloaks with pinched triangular and semi-circular shapes, respectively. For the latter, we delved into 3 types of transformations: linear ($C_1$), quadratic ($C_2$) and cubic ($C_3$) and we compared their cloaking performance via FE harmonic simulations computing the normalized transmitted displacement

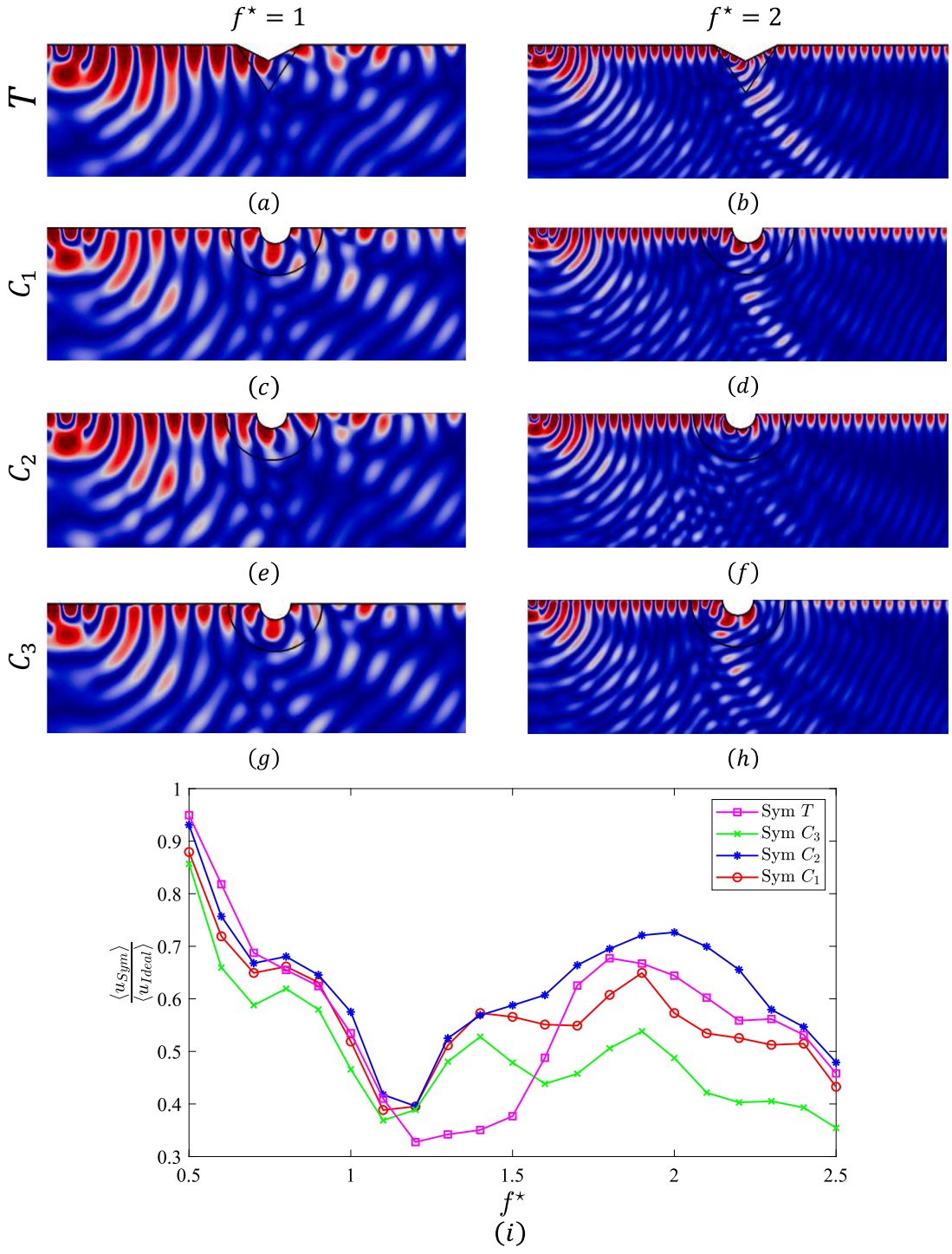


**Fig. 4.** Displacement field of the symmetrized cloaks for the $(a)-(b)$ Triangular $T$, $(c)-(d)$ Circular $C_1$, $(e)-(f)$ Circular $C_2$ and $(g)-(h)$ Circular $C_3$ class of transformations, computed at frequencies $f^\star = 1.5$ and $f^\star = 2$, respectively. $(i)$ Performance of the cloaks using the ratio of the transmitted field of the symmetrized cloak over the ideal one, calculated at normalized frequencies $f^\star = [0.5, 2.5]$.

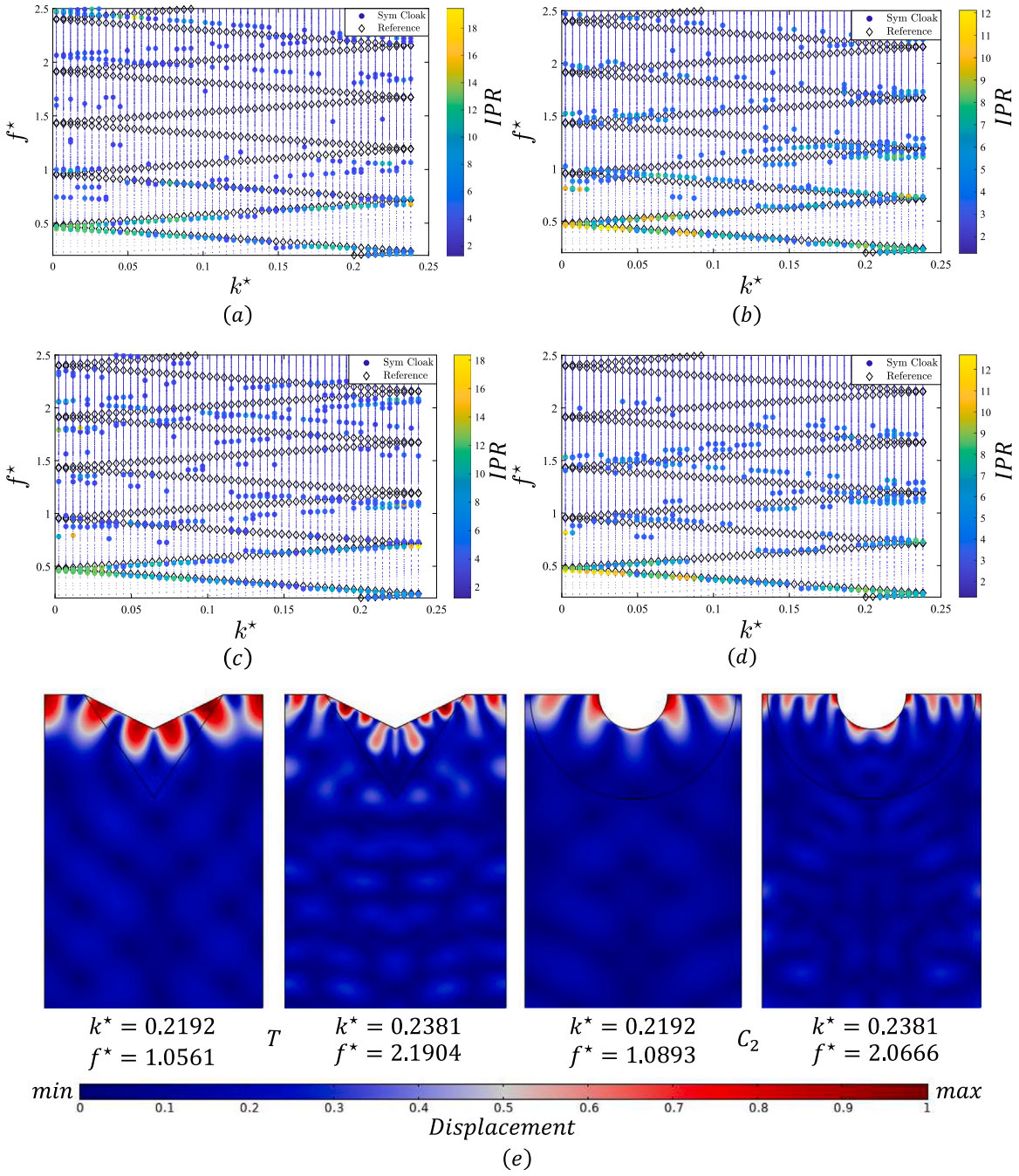


**Fig. 5.** Dispersion curves for the (*a*) Triangular $T$ and (*b*) – (*c*) – (*d*) Circular Symmetrized cloaks of $C_1$, $C_2$ and $C_3$ type of transformation, respectively, as obtained from the IPR method. (*e*) Snapshots of particular surface modes of the displacement fields, as obtained for the triangular $T$ (Left) and the Circular $C_2$ (Right) symmetrized cloaks, respectively.

field in each case. We found that a symmetrized semi-circular cloak obtained from a quadratic ($C_2$) transformation provided the best approximation of the ideal one. Additionally, we conducted dispersive analyses and employed the inverse participation ratio (IPR) as a tool to identify the surface modes among all the wave solutions. Again, we compared the results obtained for the ideal and the symmetrized scenarios and found that the $C_2$ transformation was able to support the propagation of the highest number of surface modes in comparison with all the other types of transformations. As a further proof, we discussed the value of the ratio $D^{C_i}$ and addressed its connection with the performance of the symmetrized cloak by computing its mean value with respect to the

parameter $r$. The results converged with the findings of the time-harmonic numerical simulations and the dispersive properties of the cloaks, concluding that the quadratic $C_2$ transformation displayed the best overall cloaking protection.

We stress that a classical homogenization procedure could be implemented to mimic the now symmetric, yet anisotropic behavior of the cloaks via isotropic layered media, providing a feasible protection from incident Rayleigh waves. Finally, since experiments on elastodynamic cloaking are scarce and only recently Xu et al. (2020) made the first physical realization of a polar cloak that provided shielding from static loads, we hope this study could pave the way towards more experimental validation for cloaking from surface elastic waves.

## Declaration of competing interest

The authors declare that they have no known competing financial interests or personal relationships that could have appeared to influence the work reported in this paper.

## Acknowledgments

This project has received funding from the European Union's Horizon 2020 research and innovation programme under the Marie Sklodowska Curie grant agreement No 813424.

## Appendix. Transformations with offset parameter $\epsilon$.

In this section we present the so-called Kohn's transformation (Kohn et al., 2014), which amounts to transforming the region $\epsilon \le R \le R_o$ to the cloaking region $r_i \le r \le r_o$, where $\epsilon$ is a small positive number introduced to remove the singularity at the origin. In addition, for the $C_1^\epsilon$ type transformation we provide the more general scenario, which is parametric with respect to $N$:

$$\Xi^{C_1^\epsilon(N)} : \begin{cases} r = \sqrt[N]{\frac{b^N-a^N}{b^N-\epsilon^N} R^N + a^N - \epsilon^N \frac{b^N-a^N}{b^N-\epsilon^N}} & 0 \le R \le R_o \\ \theta = \Theta \end{cases} \tag{30}$$

Note that when $\epsilon = 0$, for $N = 1$ in Eq. (30) we obtain the classical "Pendry" transformation of Eq. (11). The case of $N = 2$ has been used in Liu and Zhu (2019) and Zareei and Alam (2017) for cloaking of elastic plates and in Zareei and Alam (2015) for cloaking of shallow water waves, and has the special property that its determinant $det(\mathbf{F}^{C_1})$ is constant.

In a similar fashion, the general $C_2^\epsilon$ type of transformation is given by:

$$\Xi^{C_2^\epsilon} : \begin{cases} r = A_2^\epsilon R^2 + A_1^\epsilon R + A_0^\epsilon & 0 \le R \le R_o \\ \theta = \Theta \end{cases} \tag{31}$$

where

$$A_2^\epsilon = \frac{a-e}{(b-e)^2}, \quad A_1^\epsilon = -\frac{2\,b\,(a-e)-(b-e)^2}{(b-e)^2}, \quad A_0^\epsilon = \frac{b^2\,(a-e)}{(b-e)^2} \tag{32}$$

Finally the $C_3^\epsilon$ reads:

$$\Xi^{C_3^\epsilon} : \begin{cases} r = B_3^\epsilon R^3 + B_2^\epsilon R^2 + B_1^\epsilon R + B_0^\epsilon & 0 \le R \le R_o \\ \theta = \Theta \end{cases} \tag{33}$$

where

$$B_3^\epsilon = 2\frac{(a-\epsilon)}{(b-e)^3}, \quad B_2^\epsilon = \frac{3\,(b+\epsilon)\,(\epsilon-a)}{(b-\epsilon)^3}, \quad B_1^\epsilon = \frac{b^3-3\,b^2\,\epsilon-3\,b\,\epsilon^2+6\,a\,b\,\epsilon-\epsilon^3}{(b-\epsilon)^3}, \quad B_0^\epsilon = \frac{b^2\,(a-\epsilon)\,(b-3\,\epsilon)}{(b-\epsilon)^3}, \tag{34}$$

Note that when $\epsilon = 0$, Eqs. (31)–(34) reduce to Eqs. (11)–(15).

## References

Barnwell, E. G., Parnell, W. J., & David Abrahams, I. (2016). Antiplane elastic wave propagation in pre-stressed periodic structures; tuning, band gap switching and invariance. *Wave Motion*, *63*, 98–110. http://dx.doi.org/10.1016/j.wavemoti.2016.02.001, URL https://www.sciencedirect.com/science/article/pii/S0165212516000111.

Brûlé, S., Javelaud, E. H., Enoch, S., & Guenneau, S. (2014). Experiments on seismic metamaterials: Molding surface waves. *Physical Review Letters*, *112*, Article 133901. http://dx.doi.org/10.1103/PhysRevLett.112.133901, URL https://link.aps.org/doi/10.1103/PhysRevLett.112.133901.

Brûlé, S., Javelaud, E. H., Enoch, S., & Guenneau, S. (2017). Flat lens effect on seismic waves propagation in the subsoil. *Scientific Reports*, *7*, 2045–2322. http://dx.doi.org/10.1038/s41598-017-17661-y.

Brun, M., & Guenneau, S. (2023). Transformation design of in-plane elastic cylindrical cloaks, concentrators and lenses. *Wave Motion*, Article 103124.

Brun, M., Guenneau, S., & Movchan, A. B. (2009). Achieving control of in-plane elastic waves. *Applied Physics Letters*, *94*(6), Article 061903. http://dx.doi.org/10.1063/1.3068491.

Chatzopoulos, Z., Palermo, A., Guenneau, S., & Marzani, A. (2022). Cloaking strategy for Love waves. *Extreme Mechanics Letters*, *50*, Article 101564. http://dx.doi.org/10.1016/j.eml.2021.101564, URL https://www.sciencedirect.com/science/article/pii/S2352431621002297.

Chen, Y., Nassar, H., & Huang, G. (2021). Discrete transformation elasticity: An approach to design lattice-based polar metamaterials. *International Journal of Engineering Science*, *168*, Article 103562. http://dx.doi.org/10.1016/j.ijengsci.2021.103562, URL https://www.sciencedirect.com/science/article/pii/S0020722521001063.

Colombi, A., Roux, P., Guenneau, S., Gueguen, P., & Craster, R. V. (2016). Forests as a natural seismic metamaterial: Rayleigh wave bandgaps induced by local resonances. *Scientific Reports*, *6*, 2045–2322. http://dx.doi.org/10.1038/srep19238.

Colombi, A., Zaccherini, R., Aguzzi, G., Palermo, A., & Chatzi, E. (2020). Mitigation of seismic waves: Metabarriers and metafoundations bench tested. *Journal of Sound and Vibration*, *485*, Article 115537. http://dx.doi.org/10.1016/j.jsv.2020.115537, URL https://www.sciencedirect.com/science/article/pii/S0022460X20303692.

Colquitt, D., Brun, M., Gei, M., Movchan, A., Movchan, N., & Jones, I. (2014). Transformation elastodynamics and cloaking for flexural waves. *Journal of the Mechanics and Physics of Solids*, *72*, 131–143. http://dx.doi.org/10.1016/j.jmps.2014.07.014, URL https://www.sciencedirect.com/science/article/pii/S0022509614001586.

Craster, R., Diatta, A., Guenneau, S., & Hutridurga, H. (2021). On near-cloaking for linear elasticity. *Multiscale Modeling and Simulation*, *19*(2), 633–664.

Diatta, A., Kadic, M., Wegener, M., & Guenneau, S. (2016). Scattering problems in elastodynamics. *Physical Review B*, *94*, Article 100105. http://dx.doi.org/10.1103/PhysRevB.94.100105, URL https://link.aps.org/doi/10.1103/PhysRevB.94.100105.

Dubois, M., Etaix, N., Farhat, M., Enoch, S., Guenneau, S., Ing, R.-K., et al. (2012). Flat lens for Lamb waves focusing. In S. F. d'Acoustique (Ed.), *Acoustics 2012*. URL https://hal.science/hal-00810650.

Evers, F., & Mirlin, A. D. (2000). Fluctuations of the inverse participation ratio at the Anderson transition. *Physical Review Letters*, *84*, 3690–3693. http://dx.doi.org/10.1103/PhysRevLett.84.3690, URL https://link.aps.org/doi/10.1103/PhysRevLett.84.3690.

Farhat, M., Guenneau, S., & Enoch, S. (2009). Ultrabroadband elastic cloaking in thin plates. *Physical Review Letters*, *103*, Article 024301. http://dx.doi.org/10.1103/PhysRevLett.103.024301, URL https://link.aps.org/doi/10.1103/PhysRevLett.103.024301.

Frenzel, T., Kadic, M., & Wegener, M. (2017). Three-dimensional mechanical metamaterials with a twist. *Science*, *358*(6366), 1072–1074. http://dx.doi.org/10.1126/science.aao4640, URL https://www.science.org/doi/abs/10.1126/science.aao4640.

Huang, J., & Shi, Z. (2013). Attenuation zones of periodic pile barriers and its application in vibration reduction for plane waves. *Journal of Sound and Vibration*, *332*(19), 4423–4439. http://dx.doi.org/10.1016/j.jsv.2013.03.028, URL https://www.sciencedirect.com/science/article/pii/S0022460X13002885.

Jin, Y., Pennec, Y., Bonello, B., Honarvar, H., Dobrzynski, L., Djafari-Rouhani, B., et al. (2021). Physics of surface vibrational resonances: Pillared phononic crystals, metamaterials, and metasurfaces. *Reports on Progress in Physics*, *84*(8), Article 086502.

Kadic, M., Bückmann, T., Stenger, N., Thiel, M., & Wegener, M. (2012). On the practicability of pentamode mechanical metamaterials. *Applied Physics Letters*, *100*(19), Article 191901. http://dx.doi.org/10.1063/1.4709436.

Khlopotin, A., Olsson, P., & Larsson, F. (2015). Transformational cloaking from seismic surface waves by micropolar metamaterials with finite couple stiffness. *Wave Motion*, *58*, 53–67.

Kohn, R. V., Lu, J., Schweizer, B., & Weinstein, M. I. (2014). A variational perspective on cloaking by anomalous localized resonance. *Communications in Mathematical Physics*, *328*, 1–27. http://dx.doi.org/10.1007/s00220-014-1943-y.

Liu, Z., Qin, K.-Q., & Yu, G.-L. (2020). Partially embedded gradient metabarrier: Broadband shielding from seismic Rayleigh waves at ultralow frequencies. *Journal of Engineering Mechanics*, *146*(5), Article 04020032. http://dx.doi.org/10.1061/(ASCE)EM.1943-7889.0001752.

Liu, C.-X., & Yu, G.-L. (2022). Inverse design of locally resonant metabarrier by deep learning with a rule-based topology dataset. *Computer Methods in Applied Mechanics and Engineering*, *394*, Article 114925. http://dx.doi.org/10.1016/j.cma.2022.114925, URL https://www.sciencedirect.com/science/article/pii/S0045782522001980.

Liu, M., & Zhu, W. (2019). Nonlinear transformation-based broadband cloaking for flexural waves in elastic thin plates. *Journal of Sound and Vibration*, *445*, 270–287. http://dx.doi.org/10.1016/j.jsv.2018.12.025, URL https://www.sciencedirect.com/science/article/pii/S0022460X18308514.

Maurel, A., Marigo, J.-J., Pham, K., & Guenneau, S. (2018). Conversion of Love waves in a forest of trees. *Physical Review B*, *98*, Article 134311. http://dx.doi.org/10.1103/PhysRevB.98.134311, URL https://link.aps.org/doi/10.1103/PhysRevB.98.134311.

Meirbekova, B., & Brun, M. (2020). Control of elastic shear waves by periodic geometric transformation: cloaking, high reflectivity and anomalous resonances. *Journal of the Mechanics and Physics of Solids*, *137*, Article 103816.

Meng, L., Cheng, Z., & Shi, Z. (2020). Vibration mitigation in saturated soil by periodic pile barriers. *Computers and Geotechnics*, *117*, Article 103251. http://dx.doi.org/10.1016/j.compgeo.2019.103251, URL https://www.sciencedirect.com/science/article/pii/S0266352X19303155.

Milton, G. W. (2002). *The theory of composites*. Cambridge University Press.

Milton, G. W., Briane, M., & Harutyunyan, D. (2017). On the possible effective elasticity tensors of 2-dimensional and 3-dimensional printed materials. *Mathematics and Mechanics of Complex Systems*, *5*, 4194. http://dx.doi.org/10.2140/memocs.2017.5.41.

Milton, G. W., Briane, M., & Willis, J. R. (2006). On cloaking for elasticity and physical equations with a transformation invariant form. *New Journal of Physics*, *8*(10), 248. http://dx.doi.org/10.1088/1367-2630/8/10/248.

Monthus, C., & Garel, T. (2010). Anderson localization of phonons in dimension $d = 1, 2, 3$: Finite-size properties of the inverse participation ratios of eigenstates. *Physical Review B*, *81*, Article 224208. http://dx.doi.org/10.1103/PhysRevB.81.224208, URL https://link.aps.org/doi/10.1103/PhysRevB.81.224208.

Muhammad, Lim, C., & Kamil Żur, K. (2021). Wide Rayleigh waves bandgap engineered metabarriers for ground born vibration attenuation. *Engineering Structures*, *246*, Article 113019. http://dx.doi.org/10.1016/j.engstruct.2021.113019, URL https://www.sciencedirect.com/science/article/pii/S0141029621011615.

Murphy, N. C., Wortis, R., & Atkinson, W. A. (2011). Generalized inverse participation ratio as a possible measure of localization for interacting systems. *Physical Review B*, *83*, Article 184206. http://dx.doi.org/10.1103/PhysRevB.83.184206, URL https://link.aps.org/doi/10.1103/PhysRevB.83.184206.

Nassar, H., Chen, Y. Y., & Huang, G. L. (2018). A degenerate polar lattice for cloaking in full two-dimensional elastodynamics and statics. *Proceedings of the Royal Society A: Mathematical, Physical and Engineering Sciences*, *474*(2219), Article 20180523. http://dx.doi.org/10.1098/rspa.2018.0523, URL https://royalsocietypublishing.org/doi/abs/10.1098/rspa.2018.0523.

Nassar, H., Chen, Y., & Huang, G. (2019). Isotropic polar solids for conformal transformation elasticity and cloaking. *Journal of the Mechanics and Physics of Solids*, *129*, 229–243. http://dx.doi.org/10.1016/j.jmps.2019.05.002, URL https://www.sciencedirect.com/science/article/pii/S0022509619302169.

Nassar, H., Chen, Y. Y., & Huang, G. L. (2020). Polar metamaterials: A new outlook on resonance for cloaking applications. *Physical Review Letters*, *124*, Article 084301. http://dx.doi.org/10.1103/PhysRevLett.124.084301, URL https://link.aps.org/doi/10.1103/PhysRevLett.124.084301.

Norris, A. N., & Parnell, W. J. (2012). Hyperelastic cloaking theory: transformation elasticity with pre-stressed solids. *Proceedings of the Royal Society A: Mathematical, Physical and Engineering Sciences*, *468*(2146), 2881–2903. http://dx.doi.org/10.1098/rspa.2012.0123, URL https://royalsocietypublishing.org/doi/abs/10.1098/rspa.2012.0123.

Norris, A., & Shuvalov, A. (2011). Elastic cloaking theory. *Wave Motion*, *48*(6), 525–538. http://dx.doi.org/10.1016/j.wavemoti.2011.03.002, Special issue on cloaking of wave motion. URL https://www.sciencedirect.com/science/article/pii/S0165212511000357.

Palermo, A., Krödel, S., Marzani, A., & Daraio, C. (2016). Engineered metabarrier as shield from seismic surface waves. *Scientific Reports*, *6*, 2045–2322. http://dx.doi.org/10.1038/srep39356.

Palermo, A., Krödel, S., Matlack, K. H., Zaccherini, R., Dertimanis, V. K., Chatzi, E. N., et al. (2018). Hybridization of guided surface acoustic modes in unconsolidated granular media by a resonant metasurface. *Physical Review A*, *9*(5), Article 054026.

Palermo, A. (2018). Control of Love waves by resonant metasurfaces. *Scientific Reports*, *8*, 7234. http://dx.doi.org/10.1038/s41598-018-25503-8.

Parnell, W. J. (2012). Nonlinear pre-stress for cloaking from antiplane elastic waves. *Proceedings of the Royal Society A: Mathematical, Physical and Engineering Sciences*, *468*(2138), 563–580. http://dx.doi.org/10.1098/rspa.2011.0477, URL https://royalsocietypublishing.org/doi/abs/10.1098/rspa.2011.0477.

Parnell, W. J., & Shearer, T. (2013). Antiplane elastic wave cloaking using metamaterials, homogenization and hyperelasticity. *Wave Motion*, *50*(7), 1140–1152. http://dx.doi.org/10.1016/j.wavemoti.2013.06.006, Advanced modelling of wave propagation in solids. URL https://www.sciencedirect.com/science/article/pii/S0165212513001157.

Pu, X., & Shi, Z. (2018). Surface-wave attenuation by periodic pile barriers in layered soils. *Construction and Building Materials*, *180*, 177–187. http://dx.doi.org/10.1016/j.conbuildmat.2018.05.264, URL https://www.sciencedirect.com/science/article/pii/S0950061818313485.

Pu, X., & Shi, Z. (2019). Periodic pile barriers for Rayleigh wave isolation in a poroelastic half-space. *Soil Dynamics and Earthquake Engineering*, *121*, 75–86. http://dx.doi.org/10.1016/j.soildyn.2019.02.029, URL https://www.sciencedirect.com/science/article/pii/S0267726118312739.

Quadrelli, D. E., Craster, R., Kadic, M., & Braghin, F. (2021). Elastic wave near-cloaking. *Extreme Mechanics Letters*, *44*, Article 101262.

Sklan, S. R., Pak, R. Y. S., & Li, B. (2018). Seismic invisibility: elastic wave cloaking via symmetrized transformation media. *New Journal of Physics*, *20*(6), Article 063013. http://dx.doi.org/10.1088/1367-2630/aac7ab.

Stenger, N., Wilhelm, M., & Wegener, M. (2012). Experiments on elastic cloaking in thin plates. *Physical Review Letters*, *108*, Article 014301. http://dx.doi.org/10.1103/PhysRevLett.108.014301, URL https://link.aps.org/doi/10.1103/PhysRevLett.108.014301.

Tang, K., Luz, E., Amram, D., Kadysz, L., Guenneau, S., & Sebbah, P. (2023). Dynamic cloaking of a diamond-shaped hole in elastic plate. *Applied Physics Letters*, *122*(1), Article 011701. http://dx.doi.org/10.1063/5.0123575.

Tsukerman, E. (2017). Inverse participation ratios in the XX spin chain. *Physical Review B*, *95*, Article 115121. http://dx.doi.org/10.1103/PhysRevB.95.115121, URL https://link.aps.org/doi/10.1103/PhysRevB.95.115121.

Wegner, F. (1980). Inverse participation ratio in $2+\epsilon$ dimensions. *Zeitschrift für Physik B Condensed Matter*, *36*, 270–287. http://dx.doi.org/10.1007/BF01325284.

Wu, Q., & Huang, G. (2022). Omnidirectional wave polarization manipulation in isotropic polar solids. *International Journal of Solids and Structures*, *241*, Article 111481. http://dx.doi.org/10.1016/j.ijsolstr.2022.111481, URL https://www.sciencedirect.com/science/article/pii/S0020768322000440.

Xiang, Z., & Yao, R. (2016). Realizing the willis equations with pre-stresses. *Journal of the Mechanics and Physics of Solids*, *87*, 1–6. http://dx.doi.org/10.1016/j.jmps.2015.10.010, URL https://www.sciencedirect.com/science/article/pii/S002250961530212X.

Xu, X., Wang, C., Shou, W., Du, Z., Chen, Y., Li, B., et al. (2020). Physical realization of elastic cloaking with a polar material. *Physical Review Letters*, *124*, Article 114301. http://dx.doi.org/10.1103/PhysRevLett.124.114301, URL https://link.aps.org/doi/10.1103/PhysRevLett.124.114301.

Zareei, A., & Alam, M.-R. (2015). Cloaking in shallow-water waves via nonlinear medium transformation. *Journal of Fluid Mechanics*, *778*, 273–287. http://dx.doi.org/10.1017/jfm.2015.350.

Zareei, A., & Alam, M.-R. (2017). Broadband cloaking of flexural waves. *Physical Review E*, *95*, Article 063002. http://dx.doi.org/10.1103/PhysRevE.95.063002, URL https://link.aps.org/doi/10.1103/PhysRevE.95.063002.

Zhang, H., Chen, Y., Liu, X., & Hu, G. (2020). An asymmetric elastic metamaterial model for elastic wave cloaking. *Journal of the Mechanics and Physics of Solids*, *135*, Article 103796. http://dx.doi.org/10.1016/j.jmps.2019.103796, URL https://www.sciencedirect.com/science/article/pii/S0022509619308762.

Zhang, P., & Parnell, W. J. (2018). Hyperelastic antiplane ground cloaking. *The Journal of the Acoustical Society of America*, *143*(5), 2878–2885. http://dx.doi.org/10.1121/1.5036629.

Zhao, S., Chen, J., Chang, Z., & Huang, G. (2023). Microstructure realization of a lattice-based polar solid for arbitrary elastic waveguiding. *Journal of the Mechanics and Physics of Solids*, *173*, Article 105226. http://dx.doi.org/10.1016/j.jmps.2023.105226, URL https://www.sciencedirect.com/science/article/pii/S0022509623000303.